

Article pubs.acs.org/JCTC

PNO++: Perturbed Pair Natural Orbitals for Coupled Cluster Linear **Response Theory**

Ruhee D'Cunha and T. Daniel Crawford*



Cite This: J. Chem. Theory Comput. 2021, 17, 290-301



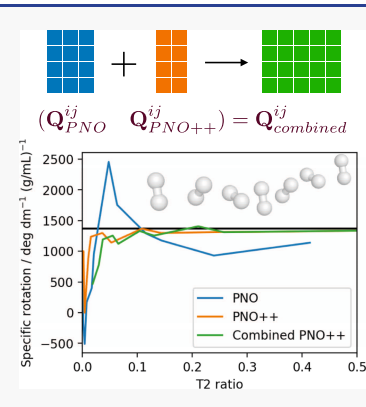
ACCESS I

III Metrics & More



Supporting Information

ABSTRACT: Reduced-scaling methods are needed to make accurate and systematically improvable coupled cluster linear response methods for the calculation of molecular properties tractable for large molecules. In this paper, we examine the perturbed pair natural orbital-based PNO++ approach that creates an orbital space optimized for response properties derived from a lower-cost field-perturbed density matrix. We analyze truncation errors in correlation energies, dynamic polarizabilities, and specific rotations from a coupled cluster singles and doubles (CCSD) reference. We find that incorporating a fixed number of orbitals from the pair natural orbital (PNO) space into the PNO++ method—a new method presented here, the "combined PNO++" approach—recovers accuracy in the CCSD correlation energy while preserving the well-behaved convergence behavior of the PNO++ method for linear response properties.



1. INTRODUCTION

For molecules and materials subjected to weak electromagnetic fields, key molecular properties may be defined via timedependent perturbation theory, response theory, by orders of their component multipole operators. 1-3 Beyond "zeroth order" properties such as dipole or magnetic moments, linear, quadratic, and higher-order dynamic response functions provide computational routes to frequency-dependent polarizabilities/magnetizabilities, hyperpolarizabilities, and other mixed electric-/magnetic-field properties.4-7 The ultimate accuracy of such computations depends critically on the choice of the quantum chemical model.

Among the simplest such models is time-dependent Hartree-Fock (TDHF) (also known as the random-phase approximation (RPA)), 8,9 whose modest computational cost is offset by its lack of treatment of dynamic electron correlation effects, leading to, for example, its overestimation of electronic excitation energies. More sophisticated methods that include at least some approximation of electron correlation can provide significantly improved predictions of molecular response properties, including time-dependent density-functional theory (TDDFT),10,11 the second-order polarization propagator (SOPPA), 12,13 the algebraic diagrammatic construction (ADC), ^{14–16} etc. One of the most robust quantum chemical models is coupled cluster (CC) theory, ^{17–20} which relies on an exponential expansion of the multideterminant wave function not only to recover electron correlation effects systematically but also to ensure the correct (intensive or extensive) scaling of response properties with respect to the size of the molecular system.

The principal disadvantage of coupled cluster theory lies in its high-order polynomial scaling with system size, due to the combination of delocalized canonical molecular orbitals and electron correlation effects, which are local in nature.²¹ Efforts to reduce the cost of coupled cluster calculations have resulted in the development of several reduced-scaling methods based on orbital localization, $^{22-26}$ tensor decompositions, $^{27-32}$ and fragmentation schemes, $^{33-36}$ among others. The aim of orbital localization schemes in particular is to utilize the intrinsic sparsity in correlated wave functions to reduce the scaling of ground- and excited-state property calculations. Local correlation methods such as projected atomic orbitals (PAOs) introduced by Pulay and Saebo 21,22 and extended to coupled cluster theory by Hampel and Werner, 23 pair natural orbitals (PNOs) first pioneered by Meyer,³⁷ Edmiston and Krauss, 38,39 as well as Ahlrichs and co-workers, 40 and resurrected by Neese and co-workers, 24,41 and orbital-specific virtuals (OSVs) created more recently by Yang et al.26 introduce controllable sparsity into the wave function via orbital localization and have been successfully applied to the computation of properties related to ground-state energies without significant loss of accuracy. Though a number of local correlation schemes have been introduced for properties such as excitation energies, 42-48 due to the complexity of

Received: October 14, 2020 Published: December 22, 2020





calculations of higher-order response properties, the application of localization methods to such properties has been limited so far. $^{49-54}$

In a first application of the PNO and OSV approaches to CCSD linear response properties, McAlexander and Crawford compared the performance of three local correlation approaches (PAO, PNO, and OSV) in the calculation of response properties⁵⁵ and found that the system showed reduced sparsity in the wave function when perturbed by an external field. This resulted in increased sensitivity of the response properties to truncation of the wave function, particularly the mixed electric dipole-magnetic dipole property of specific rotation. Kumar and Crawford further explored the effects of truncation of a virtual natural orbital (NO) space on linear response properties⁵⁶ and concluded that the virtual NO space did not preserve accuracy in those properties following aggressive truncation. It was seen that the truncation of NOs contributing little to electron correlation effects corresponded to the truncation of those that were most diffuse and therefore essential for the description of fieldresponse properties. A natural alternative is to build an orbital space optimized for those properties sought. Transitionspecific virtual spaces have been built by utilizing correlated natural transition orbitals, first introduced by Høyvik, Myhre, and Koch for use with the multilevel coupled cluster scheme, and later used by Baudin and Kristensen in combination with their local framework to reduce the scaling of excitation-energy calculations. 58,59 Effective natural transition orbitals have also been constructed by Höfener and Klopper by utilizing both ground- and excited-state densities. 60 Mester, Nagy, and Kállay have combined MP2 and CIS(D) densities to produce statespecific natural orbitals and natural auxiliary functions for the computation of excitation energies. 61,62

In this work, we examine the PNO++ approach, which incorporates the external field perturbation into the density and thus the orbital space, and uses this perturbed basis throughout the calculation. We create a union of the PNO and PNO++ bases, called the "combined PNO++" basis, to accurately describe both the ground- and excited-state wave functions. We further explore the PNO++ and combined PNO++ approaches, examining the sparsity introduced by the use of the PNO++ basis, followed by the analysis of the truncation error for both correlation energies and second-order response properties, i.e., dipole polarizabilties and specific rotations. We also examine the effect of an MP2-level correction for response properties, analogous to the MP2-level external space correction commonly used in PNO-related methods.

2. THEORY AND COMPUTATIONAL DETAILS

2.1. Coupled Cluster Linear Response. Coupled cluster response theory is an accurate way to simulate the response of a molecular system to an external electromagnetic field, with the time-dependent field treated as a perturbation. The coupled cluster linear response function is the first-order term in the perturbative expansion of the time-independent operator \hat{A} in response to the external field \hat{B} , and can be expressed in terms of perturbed wave function operators, dependent on the frequency ω of the external field

$$\langle\langle \hat{A}; \, \hat{B} \rangle\rangle_{\omega} = \frac{1}{2} \hat{P}(\hat{A}(-\omega), \, \hat{B}(+\omega)) [\langle 0|(1+\hat{\Lambda})[\overline{A}, \, \hat{X}_{\omega}^{B}]|0\rangle + \langle 0|\hat{Y}_{\omega}^{B}\overline{A}|0\rangle]$$
(1)

where \hat{P} is a permutation operator that ensures that the response function is real, \bar{A} is the similarity-transformed operator, and $\hat{\Lambda}$ are the left-hand coupled cluster amplitudes. The frequency-dependent perturbed operators \hat{X}^B_ω and \hat{Y}^B_ω are obtained using sets of perturbed wave function equations for each of the Cartesian directions

$$\langle \mu | (\overline{H} - \omega I) \hat{X}_{\omega}^{B} | 0 \rangle = -\langle \mu | \overline{B} | 0 \rangle \tag{2}$$

$$\begin{split} & \langle \mu | \hat{Y}_{\omega}^{B}(\overline{H} + \omega I) | 0 \rangle \\ & = - \langle 0 | (1 + \Lambda)[\overline{B}, \tau] | \mu \rangle - \langle 0 | (1 + \Lambda)[[\overline{H}, \tau], \tau] \hat{X}_{\omega}^{B} | \mu \rangle \end{split}$$

Second-order properties, such as dynamic polarizabilities and optical rotations, are then obtained by computing molecular property tensors as the appropriate linear response functions. The polarizability tensor $\alpha(\omega)$ is computed using the electric dipole moment operator $\hat{\mu}$, and the Rosenfeld tensor $\beta(\omega)$ is computed using both the electric and magnetic dipole moment (\hat{m}) operators 3,4,66

$$\alpha(\omega) = -\langle\langle \hat{\mu}; \hat{\mu} \rangle\rangle_{\omega} \tag{4}$$

$$\beta(\omega) = \operatorname{Im}\langle\langle \hat{\mu}; \, \hat{m} \rangle\rangle_{\omega} \tag{5}$$

Coupled cluster linear response involves the solving of first the coupled-cluster amplitude and lambda equations, followed by the solving of 12 sets of perturbed amplitude equations for each wavelength of interest. The main drawback of the coupled cluster method is the high-degree polynomial scaling with the system size. Coupled-cluster singles and doubles (CCSD), used in this work, scales as $O(N^6)$, where N is a measure of the system size. This necessitates some form of reduced-scaling method to make coupled cluster viable for larger molecules.

2.2. Local Pair Natural Orbitals. The pair natural orbital (PNO) approach, resurrected by Neese et al. as local pair natural orbitals (LPNO), 24,41 is a reduced-scaling approach that relies upon the creation of a more compact virtual-orbital space using the pair density. In the LPNO-CCSD approach, the pair density \mathbf{D}^{ij} for a given pair of localized occupied orbitals ij is defined for second-order Møller–Plesset perturbation theory (MP2)^{67,68} amplitudes \mathbf{T}^{ij} as

$$\mathbf{D}^{ij} = \frac{2}{1 + \delta_{ij}} (\mathbf{T}^{ij} \tilde{\mathbf{T}}^{ij\dagger} + \mathbf{T}^{ij\dagger} \tilde{\mathbf{T}}^{ij})$$
(6)

wit

$$\tilde{\mathbf{T}}^{ij} = 2\mathbf{T}^{ij} - \mathbf{T}^{ij\dagger} \tag{7}$$

The PNO-basis Q^{ij} is obtained by diagonalizing this density:

$$\mathbf{D}^{ij}\mathbf{Q}^{ij} = \mathbf{Q}^{ij}\mathbf{n}^{ij} \tag{8}$$

A truncation is carried out by comparing the set of occupation numbers $\{\mathbf{n}^{ij}\}$ to a predetermined threshold T_{cutPNO} and discarding any virtual orbitals with occupation numbers below the threshold. A further truncation is applied by discarding weakly interacting occupied pairs using a criterion based on the semicanonical MP2 pair correlation energy for each pair, defined as

$$\epsilon_{ij} = \sum_{ijab} t_{ij}^{ab} \langle ij || ab \rangle \tag{9}$$

with localized occupied pairs ij and canonical virtual orbitals ab. The occupied pairs ij are sorted into weak and strong pairs

based on if ϵ_{ij} is lesser or greater than another fixed threshold T_{cutPairs} and weak pairs are then neglected in the calculation. The occupied space is localized using one of several mathematical criteria, which form the basis of the Boys–Foster, Pipek–Mezey, Bdmiston–Ruedenberg, Magnas-co–Perico, and von Niessen localization schemes. This localization of the occupied space is important in the truncation of weak pairs, based on the logic that two-electron integrals $\langle ij || ab \rangle$ remain small if, given that the occupied orbitals i and j are spatially distant, the overlap between the occupied—virtual pairs ia and jb is small.

The PNO-basis Q^{ij} is much more compact in terms of contributions to the correlation energy and thus can be truncated to, e.g., one-tenth of the total virtual space while preserving 99% of the correlation energy (vide infra). This aggressive truncation is an essential part of the reduced scaling of the method since a distinct set of virtual orbitals is created for every pair of occupied orbitals, and thus a large number of integrals must be constructed and stored, one set for each occupied pair. The virtual orbitals for a given pair are orthonormal within a set; however, the sets of virtual orbitals are nonorthogonal between pairs, and an overlap matrix $S^{ij, kl}$ between the pairs ij and kl must be constructed and inserted into the regular coupled cluster equations.

Since its reappearance, the LPNO method has been extended to include open-shell cases⁷⁴ as well as explicit correlation,⁷⁵ parallelization,⁷⁶ and other optimizations.^{77,78} The PNO method has also been applied to the calculation of excitation energies, ionization potentials, and electron affinities. 42-44,79-82 An application of pair natural orbitals to linear response theory by Frank and Hattig⁴⁵ led to statespecific PNOs being used to obtain excitation energies as the eigenvalues of the Jacobian. The optimized PNO method has also been extended to obtain analytic energy derivatives⁸³ leading to first-order molecular properties. McAlexander and Crawford⁵⁵ published the first application of the PNO method to second-order properties, namely dynamic polarizabilities and specific rotations; however, the three reduced-scaling methods compared in that work showed oscillations in the value of the CCSD-level optical rotation with the truncation of the virtual space and hence could not directly be used in the same way to compute these more sensitive properties.

2.3. Perturbation-Aware Densities. We see from the form of the coupled cluster linear response function $(eq\ 1)$ that the final value of the response property sought is dependent not only on the ground state of the system as defined in the coupled cluster ansatz but also on the external perturbation via the perturbed wave function amplitudes. Thus, to find a more effective compact basis in which to compute molecular properties, we modify the definition of the PNO basis to include the effect of the perturbation on the system.

As seen from previous work done in our group, ⁸⁴ the PNO+ pair density is formulated in an analogous fashion to the PNO pair density (eq 6), with the first-order perturbed amplitudes X_B^{ij} , corresponding to the perturbed wave function operators \hat{X}_{ω}^{ij} seen above, replacing the ground-state amplitudes \mathbf{T}^{ij}

$$\mathbf{D}^{ij}(B,\,\omega) = \frac{2}{1+\delta_{ij}} (\mathbf{X}_{B}^{ij}\tilde{\mathbf{X}}_{B}^{ij\dagger} + \mathbf{X}_{B}^{ij\dagger}\tilde{\mathbf{X}}_{B}^{ij})$$
(10)

with \mathbf{X}_{B}^{ij} defined similarly to eq 7.

To create a density from MP2-level calculations, first-order perturbed guess amplitudes must be created using a perturbation \overline{B} and Hamiltonian matrix elements \overline{H}_{pp} , both similarity-transformed

$$X_{ab}^{ij} = \frac{\overline{B}}{\overline{H}_{aa} + \overline{H}_{bb} - \overline{H}_{ii} - \overline{H}_{jj} + \omega}$$
(11)

This is the usual form of the guess amplitudes in the coupled cluster linear response equations above (eq 2). The Hamiltonian matrix elements are given in eqs 12a and 12b in terms of Fock matrix elements f_{pq} , MP2 amplitudes t^{ij}_{ab} , and antisymmetrized two-electron integrals $\langle ij || ab \rangle$.

$$\bar{H}_{ii} = f_{ii} + \frac{1}{2} t_{ef}^{in} \langle in || ef \rangle$$
(12a)

$$\bar{H}_{aa} = f_{aa} - \frac{1}{2} t_{fa}^{mn} \langle mn || fa \rangle$$
(12b)

Similarity-transformed Hamiltonian matrix elements are found by applying the Baker–Campbell–Hausdorff expansion to the second-quantized Hamiltonian and setting the terms in the final expression which contain t_a^i to zero. Once the perturbation-aware pair density $\mathbf{D}^{ij}(B,\omega)$ is created, it can be used to create the PNO++ basis in an identical way to the PNO basis, and thus a similar approach is used to reduce the scaling of the coupled cluster linear response equations.

2.4. MP2-Level Correction. The MP2-level perturbative correction added to the LPNO-CCSD correlation energy, as described in ref 24, constitutes a substantial improvement to the value of the correlation energy at larger truncations. The correction is defined as the difference between the MP2-level correlation energy of the full, untruncated space and the correlation energy of the truncated space

$$\Delta_{\text{MP2}} = E_{\text{MP2}}^{\text{full}} - E_{\text{MP2}}^{\text{PNO}} \tag{13}$$

This correction is then added to the LPNO-CCSD correlation energy to obtain corrected energy values. To improve the PNO ++-CCSD property values at large truncations in a similar way, MP2-level corrections to the PNO++ polarizability and specific rotation values are defined as

$$\Delta \alpha_{\text{MP2}} = \alpha_{\text{MP2}}^{\text{full}} - \alpha_{\text{MP2}}^{\text{PNO} + +} \tag{14}$$

$$\Delta \beta_{\mathrm{MP2}} = \beta_{\mathrm{MP2}}^{\mathrm{full}} - \beta_{\mathrm{MP2}}^{\mathrm{PNO} + +} \tag{15}$$

However, due to the absence of an MP2-level linear response analogue to the MP2 correlation energy, MP2-level properties are defined as the linear response function containing MP2-level amplitudes, as well as perturbed X_{ω} and Y_{ω} amplitudes derived from these using eqs 12a and 12b.

The linear response function contains a frequency-dependence that is incorporated via the dependence of the perturbed X_{ω} and Y_{ω} amplitudes on the frequency of the external field. When computing the MP2-level correction in the modified-velocity gauge, we select the zero-frequency correction, since the difference in the frequency-dependent and zero-frequency corrections is minimal.

2.5. Computational Details. To check the accuracy of our method without a full production-level implementation involving the creation and storage of PNO-basis integrals and overlap matrices, a local filter approach was used, as used previously for PAO calculations, ²³ and described in ref 55. To begin, the occupied space was localized using the Pipek—

Figure 1. Systems used in this work. (a) $(H_2)_7$ helix, (b) H_2O_2 , and (c) (P)-1,3-dimethylallene (DMA).

Mezey localization criterion, 70 due to its relative efficiency and accuracy. These orbitals were then used to run a canonical CCSD linear response calculation, with a simulation code applied at each iteration. The simulation code transforms the residuals \mathbf{R}^{ij} obtained at each iteration of the coupled cluster amplitude equations to first, the PNO basis, obtained as \mathbf{Q}^{ij} in eq. 8, and then to the semicanonical basis in which the virtual block of the Fock matrix is diagonal

$$\bar{\mathbf{R}}^{ij} = \mathbf{L}^{ij\dagger} \mathbf{Q}^{ij\dagger} \mathbf{R}^{ij} \mathbf{Q}^{ij} \mathbf{L}^{ij} \tag{16}$$

where \mathbf{L}^{ij} is the result of the diagonalization of the virtual block of the Fock matrix in the PNO basis, \mathbf{F}^{ij}

$$\mathbf{F}^{ij}\mathbf{L}^{ij} = \mathbf{L}^{ij}\overline{\boldsymbol{\epsilon}}^{ij} \tag{17}$$

The denominator consisting of diagonal Fock matrix elements f_{ii} and semicanonical orbital energies $\overline{\epsilon}_a$ is then applied to obtain the increment in the local basis, which is then converted back into the canonical MO basis.

$$\bar{\Delta}_{ab}^{ij} = \frac{\bar{R}_{ab}^{ij}}{f_{ii} + f_{jj} - \bar{\epsilon}_a - \bar{\epsilon}_b}$$
(18)

$$\mathbf{\Delta}^{ij} = \mathbf{Q}^{ij} \mathbf{L}^{ij} \overline{\mathbf{\Delta}}^{ij} \mathbf{L}^{ij\dagger} \mathbf{Q}^{ij\dagger} \tag{19}$$

Thus, the final increment, containing no nonlocal contributions, is added to the previous iteration's coupled cluster amplitudes and the loss in accuracy in the converged energy values can be obtained with minimal alteration to the existing coupled cluster response code. A similar procedure is applied to the $\hat{\Lambda}$ and the perturbed wave function equations, to obtain the loss in accuracy in the converged property values.

The PNO and PNO++ pair densities were created using the forms from eqs 6 and 10. For the PNO++ density, since the perturbed wave function depends on the direction of the external field relative to the molecule, a separate density was created for each of the Cartesian directions. The densities were then averaged to obtain a single density for natural orbitals. This density was then diagonalized to obtain the PNO++ basis, which was then truncated using a threshold $T_{\rm cutPNO++}$. To create a combined space, the PNO and PNO++ spaces were both created by individually diagonalizing the PNO and PNO++ pair density matrices, followed by truncation using two separate thresholds, $T_{\rm cutPNO}$ and $T_{\rm cutPNO++}$. The spaces were then concatenated as in eq 20, and a QR decomposition was used to orthogonalize the space that remained.

$$\mathbf{Q}_{\text{combined}}^{ij} = [\mathbf{Q}_{\text{PNO}}^{ij} \cap \mathbf{Q}_{\text{PNO}++}^{ij}]$$
(20)

A few test systems were used to clearly see the convergence of the method for both optimally localized and general molecular systems. $(H_2)_n$ systems, with n = 4, 5, 6, 7, were used as a best-case scenario for the MO localization, as well as having large values of optical rotation in the arrangement chosen (Figure 1). The $(H_2)_n$ systems were also organized to lie along the Y-axis, to maximize the directionality of the perturbed wave

function. As more general small-molecule systems, H_2O_2 and (P)-1,3-dimethylallene (DMA) were used. The aug-cc-pVDZ basis set was used for the correlation energy, dynamic polarizability, and specific rotation calculations. Specific rotations and dynamic polarizabilities were computed at the sodium D-line wavelength, 589 nm.

3. RESULTS AND DISCUSSION

3.1. Amplitude Sparsity. Figure 2 shows the distribution of the converged CCSD T_2 amplitudes for a linear system, 1-

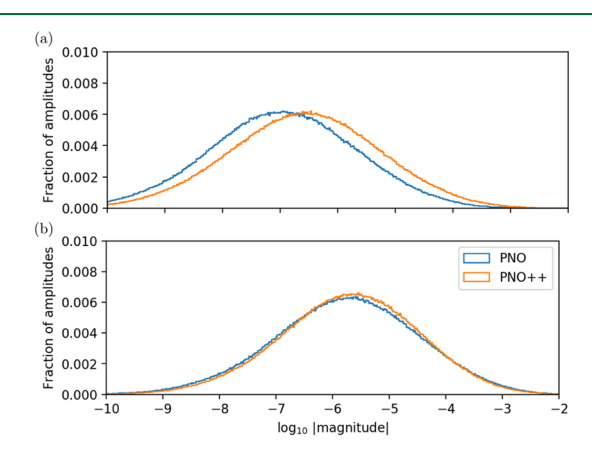


Figure 2. Fractions of (a) unperturbed and (b) perturbed CCSD wave function amplitudes for the PNO space (blue) and the PNO++ space (orange) as a function of their magnitude for 1-fluoro-heptane using the 6-31G basis set.

fluoro-heptane, as well as the converged CCSD perturbed wave function amplitudes X_2^{μ} that contribute to the linear response function. The distribution was created by localizing the occupied space using the Pipek-Mezey localization scheme, followed by localization of the virtual space into the PNO and PNO++ spaces. These spaces were not truncated to analyze the sparsity introduced by each method. We may use the magnitude distribution of wave function amplitudes as a measure of the sparsity introduced by the localization of the virtual space. Such sparsity in the wave function should, in principle, allow a more aggressive truncation threshold without a commensurate loss in accuracy. However, we note that our system of truncation using occupation numbers does not necessarily imply removal of amplitudes of small magnitudes, but instead, amplitudes of any magnitude may be removed. Amplitudes with values below 10⁻¹⁰, the coupled cluster convergence threshold, are not shown, to focus on the most significant values.

The sparsity introduced by the PNO approach was contrasted by McAlexander and Crawford⁵⁵ with the projected atomic orbital^{21–23} (PAO) and orbital-specific virtual²⁶ (OSV) approaches, and it was concluded that the PNO distribution contained the most sparsity, especially for the unperturbed

amplitudes. Figure 2a shows that the PNO++ method conserves much of this sparsity, showing an unperturbed peak within an order of magnitude of the peak for the PNO method. The perturbed amplitudes that contribute to the response equation have a right-shifted distribution with larger magnitudes compared to the unperturbed amplitudes, as seen in Figure 2b. The PNO and PNO++ spaces have very similar distributions of perturbed amplitudes and thus could be expected to show similar truncation errors; however, as seen later, the PNO++ method allows us to truncate the space more aggressively than the PNO method.

3.2. Orbital Extent. Accurate calculations of response properties require more diffuse basis functions; ⁸⁶ thus, to obtain an idea of the relative diffuseness of the orbital spaces computed using the natural orbital (NO) and perturbed natural orbital (NO++) methods, we look at the spatial extent of the virtual orbitals, defined as $\langle r^2 \rangle$, in Figure 3. Plotted

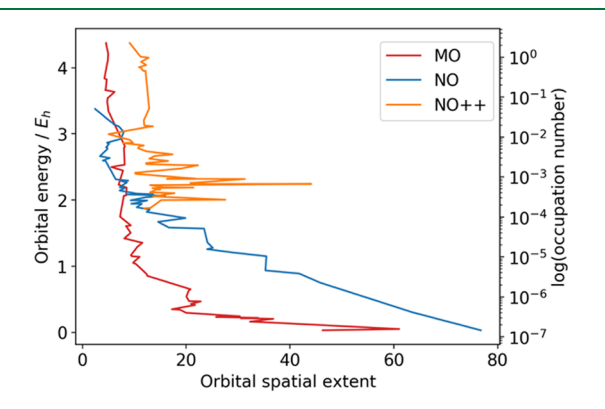


Figure 3. Orbital energies and occupation numbers plotted against orbital spatial extents for the canonical MO, PNO, and PNO++ spaces for the $\rm H_2O_2$ molecule using the 6-31G basis set.

against them are virtual-orbital energies in the case of canonical molecular orbitals (MOs) and occupation numbers on the log scale in the case of natural orbitals and perturbed natural orbitals. The natural orbitals and perturbed natural orbitals are created by diagonalizing MP2-level densities given by

$$D_{ab} = \sum_{ijc} 2t_{bc}^{ij} (2t_{ac}^{ij} - t_{ca}^{ij})$$
(21)

and

$$D_{ab}(B, \omega) = \sum_{ijc} 2x_{bc}^{ij} (2x_{ac}^{ij} - x_{ca}^{ij}) + \sum_{i} x_{i}^{a} x_{i}^{b}$$
(22)

$$x_{ab}^{ij} = \frac{\overline{B}}{\overline{H}_{aa} + \overline{H}_{bb} - \overline{H}_{ii} - \overline{H}_{jj} + \omega}$$
(23)

$$x_i^a = \frac{\overline{B}}{\overline{H}_{aa} - \overline{H}_{ii} + \omega} \tag{24}$$

The similarity-transformed \overline{H} and \overline{B} elements are formed as described in Section 2.3.

Overall, we see that the canonical MOs follow a trend of the orbitals with smaller orbital energies having the largest spatial extent. Comparing the NO space to this, we see that natural orbitals follow a similar trend, with the orbitals with the smallest occupation numbers being the most diffuse. In the usual truncation scheme, this corresponds to the most diffuse orbitals being the first ones truncated. This can explain the requirement of a large number of orbitals kept to accurately compute response properties. On the other hand, while the perturbed natural orbitals have larger magnitudes of occupation numbers, their extent lies between 5 and 25, with just one outlier. We see that these orbitals continue to be at the same diffuseness even at the larger occupation numbers that are kept as the space is truncated. This points to a more even

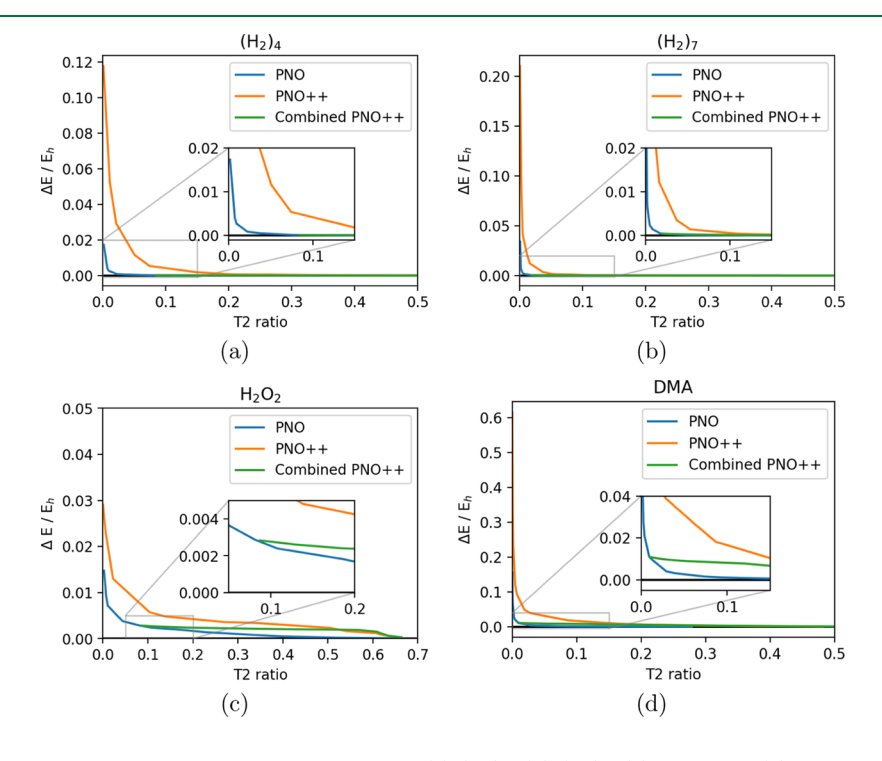


Figure 4. Truncation errors in CCSD correlation energy in Hartree for (a) $(H_2)_4$, (b) $(H_2)_7$, (c) H_2O_2 , and (d) DMA systems, computed using the aug-cc-pVDZ basis set.

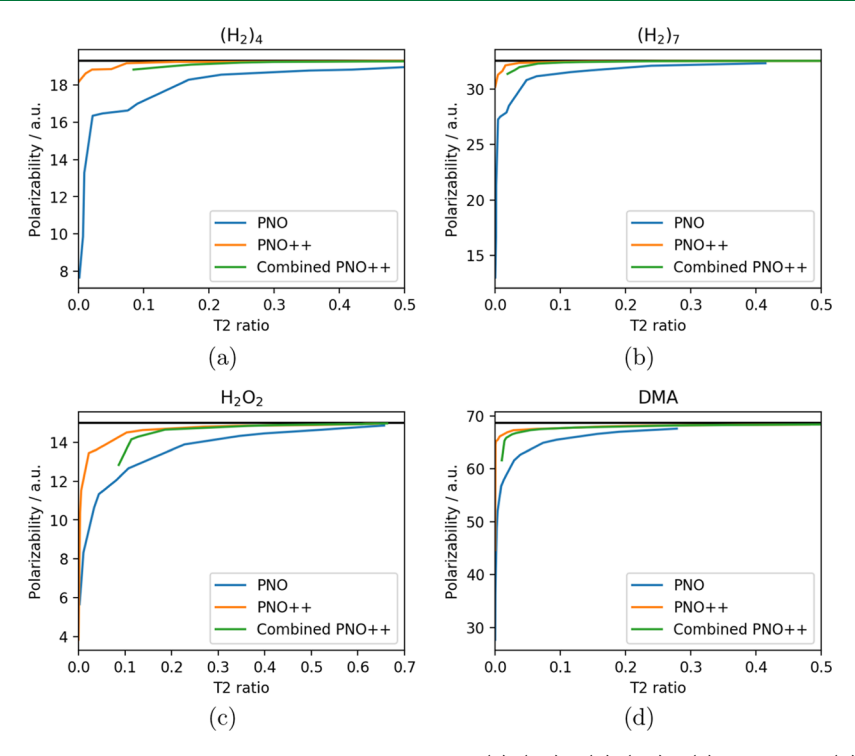


Figure 5. CCSD linear response dynamic polarizabilities at 589 nm in au for (a) $(H_2)_4$, (b) $(H_2)_7$, (c) H_2O_2 , and (d) DMA systems, computed using the aug-cc-pVDZ basis set.

distribution of the orbital extents with occupation numbers and can explain the method's improved accuracy as seen in Sections 3.3.2 and 3.3.3.

3.3. PNO++ Results. 3.3.1. Correlation Energies. CCSD correlation energies were computed for all systems using the simulation code described in Section 2.5. In Figure 4, errors in correlation energy values are plotted against the T_2 ratio, defined as the ratio of the number of wave function amplitudes present in the truncated space to the total number of wave function amplitudes in the full, untruncated space. The errors in correlation energy were computed using: $\Delta E = E_{PNO/PNO++}$ - E_{CCSD} . The T_2 ratio is used as a measure of the cost of a production-level calculation, since contractions over doubles amplitudes and two-electron integrals are the most expensive portions of a CCSD linear response calculation. Although a truncation threshold was used to remove orbitals from the calculation, an analysis using the T_2 ratio removes any ambiguity caused by the differing sparsity of the PNO and PNO++ spaces and provides a clearer picture of the computational savings obtained. The relationship between the T_2 ratio and the truncation threshold used for each method is shown in the Supporting Information (SI).

Figure 4 shows truncation errors for the smallest and largest $(H_2)_n$ systems considered, as well as H_2O_2 and DMA. The PNO++ method has a more sharply rising error with truncation as compared to the PNO method, which is seen most clearly for the larger molecules of H_2O_2 and DMA. The PNO density is created using T_2 amplitudes, while the PNO++ density is created using X_2^B amplitudes, and thus is not optimized for sparsity in the T_2 amplitudes. While the PNO++ method is optimized for response properties, it is desirable for the method to also describe the ground-state wave function in an accurate way. One method of recapturing accuracy in the correlation energy involves including both the PNO and the

PNO++ spaces in the calculation, in a combined PNO++ method as described in Section 2.3.

Figure 4 also reports a comparison of the errors in correlation energies for the PNO, PNO++, and combined PNO++ methods as a function of the T_2 ratio. The combined PNO++ method has two distinct truncation thresholds, T_{cutPNO} for the PNO space and $T_{\text{cutPNO}++}$ for the PNO++ space, and the variation of both these thresholds affects the accuracy of the method. As seen later, the variation of the perturbed threshold makes a much larger difference than the same variation of the unperturbed threshold, and thus we have selected and fixed a reasonable threshold for the PNO space (T_{cutPNO}) of 10^{-6} while varying the perturbed threshold only. This combined method introduces only a slight error at the same T_2 ratio or the same fraction of the space as compared to the original PNO method. We see larger errors for the combined method for DMA, the largest molecule we examine; however, we do not see a steep increase in the error at large truncations, in contrast to the PNO++ method. While the combined method appears to be simply creating the same space as the PNO approach, the results for the dipole polarizabilities and specific rotations in Sections 3.3.2 and 3.3.3 indicate that this is not the case. The combined space created is optimized for both correlation energies and properties.

3.3.2. Dynamic Polarizabilities. Figure 5 reports dynamic dipole polarizabilities computed at 589 nm using the PNO, PNO++, and combined PNO++ approaches as a function of the T_2 ratio. The PNO++ method shows a significant improvement over the PNO method, obtaining 99% of the CCSD reference polarizability value for our smallest system, $(H_2)_4$ at a low truncation threshold with a T_2 ratio of 0.074. A similar value requires a T_2 ratio above 0.60 when using PNOs. As the size of the $(H_2)_n$ systems increases, we see that the PNO++ method requires smaller fractions of the space to be kept to obtain 99% of the reference value, with the $(H_2)_7$

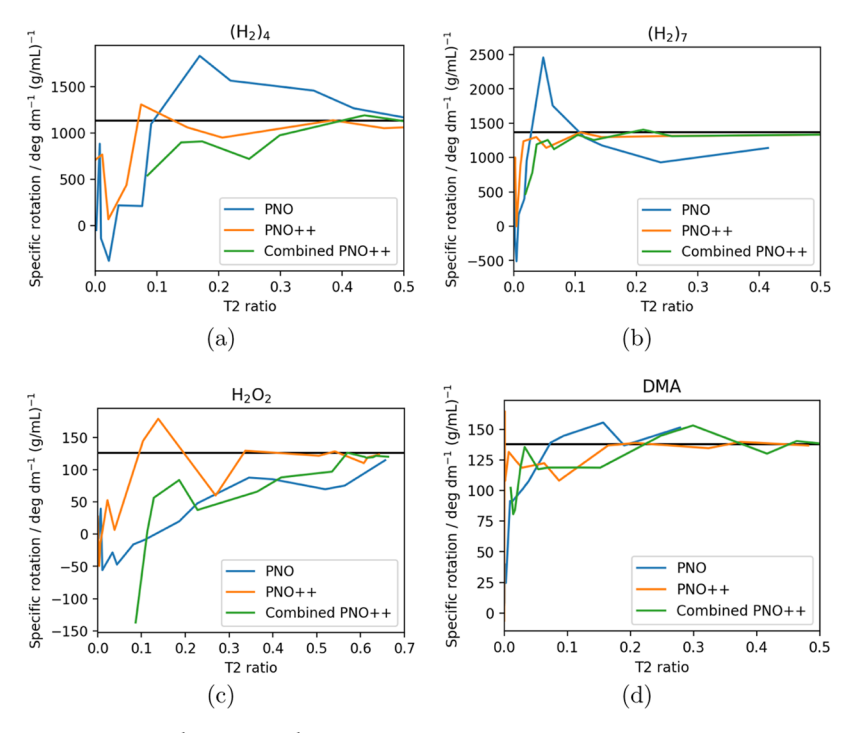


Figure 6. CCSD specific rotations in deg dm $^{-1}$ (gm/mL) $^{-1}$ at 589 nm for (a) (H₂)₄, (b) (H₂)₇, (c) H₂O₂, and (d) DMA systems, computed using the aug-cc-pVDZ basis set.

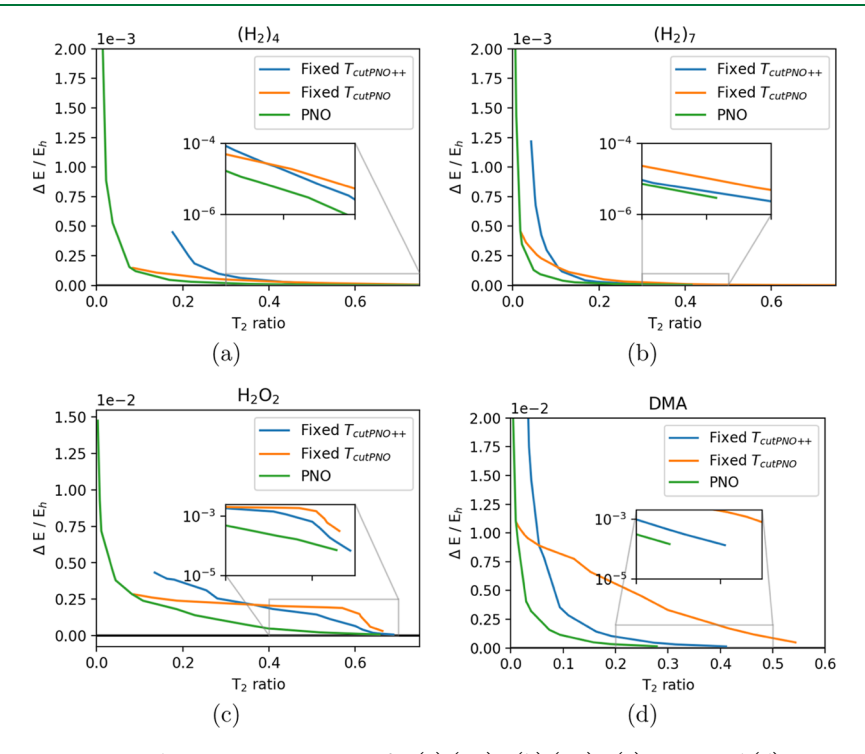


Figure 7. Truncation errors in CCSD correlation energy in Hartree for (a) $(H_2)_4$, (b) $(H_2)_7$, (c) H_2O_2 , and (d) DMA systems, computed using the aug-cc-pVDZ basis set for the PNO and PNO++ methods. Inset axes show errors on a logarithmic scale.

system requiring only 3.68% of the T_2 amplitudes needed in a conventional CCSD calculation. The data for the H_2O_2 and DMA systems also shows the PNO++ method achieving 99% accuracy at T_2 ratios of 0.61 and 0.087, respectively, while the PNO method required a T_2 ratio of 0.70 for the H_2O_2 system to achieve similar levels of accuracy and did not obtain 99% of the CCSD value at the smallest threshold used.

For all systems and methods considered, monotonic convergence toward the polarizability value was observed; albeit much more slowly for the PNO method. The combined PNO++ method, in this case, introduces an error relative to the PNO++ method alone, but the largest truncation error is still within 14% of the reference and is traded off by the improvement seen in the CCSD correlation energy in Section 3.3.1. The $T_{\rm cutPNO}$ thresholds present different T_2 ratios at the

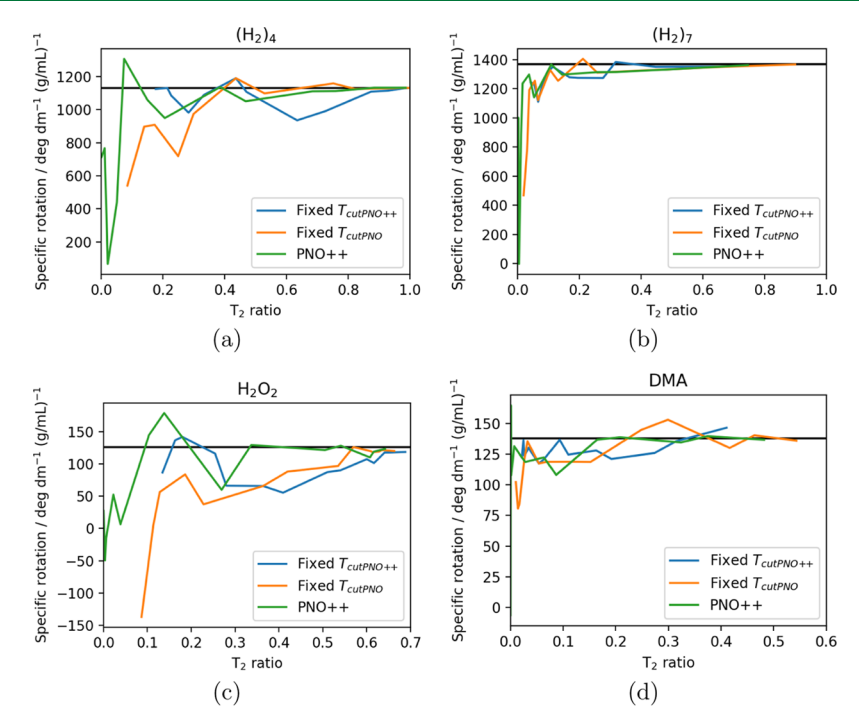


Figure 8. CCSD specific rotations in deg dm $^{-1}$ (gm/mL) $^{-1}$ at 589 nm for (a) (H $_2$) $_4$, (b) (H $_2$) $_7$, (c) H $_2$ O $_2$, and (d) DMA systems, computed using the aug-cc-pVDZ basis set.

same threshold for the different methods, since the densities are distinct and thus different numbers of amplitudes are kept. The combined PNO++ curves begin at a larger T_2 ratio due to the $T_{\rm cutPNO}$ threshold being set to 10^{-6} , with the $T_{\rm cutPNO++}$ varying.

The dynamic polarizability data suggests that the PNO++ density, created using the X_2^B amplitudes, is more efficient than the PNO density at creating a compact space with which to approximate external field-dependent properties. Combining the spaces and orthogonalizing them, as in the combined PNO++ approach, captures most of the efficiency for properties seen in the PNO++ method while also describing the ground-state wave function with higher accuracy.

3.3.3. Specific Rotations. Figure 6 shows specific rotations using the modified-velocity gauge representation of the electric dipole moment operator, computed at 589 nm using the PNO and PNO++ methods. For this and the following graphs, the electric dipole moment operator was chosen as the perturbation in the creation of the perturbed density. The use of the magnetic dipole moment operator in the perturbed density was considered; however, convergence behavior suffered (see SI for more details). For the $(H_2)_n$ systems, the behavior of the specific rotations is similar to that of the polarizabilities, in that the PNO++ method converges to within 5% of the reference value at a T_2 ratio of 0.68 for $(H_2)_4$ and 0.26 for $(H_2)_7$, while the PNO method does not seem to converge even at the fairly large T_2 ratios examined here. The DMA system also follows a similar trend, with the PNO value unconverged at a T_2 ratio of 0.48, the largest T_2 ratio considered, while the PNO++ value converges to within 5% at a T_2 ratio of 0.16. H_2O_2 exhibits the slowest convergence, with the PNO rotation value showing slow convergence, while the PNO++ method oscillates about the reference. However, the PNO++ method does remain within ±15% of the CCSD value beginning at the fairly low T_2 ratio of 0.34.

Examining Figure 6, we see that similar to the polarizability data, the combined PNO++ approach introduces an error relative to the PNO++ approach and begins at a higher T_2 ratio due to the orbitals kept from the PNO space at a $T_{\rm cutPNO}$ threshold of 10^{-6} . Unlike the polarizability, contributions to the specific rotation are not always positive but can also be negative; this means that the truncation error shows itself as an oscillation instead of approaching the reference value from the same side. This is most clearly seen in Figure 6d, the DMA system. The combined PNO++ method continues to show convergence toward the reference value below a T_2 ratio of 0.5, in contrast to the PNO method for all systems.

3.4. Combined PNO++ Method. To explore the variation in accuracy of the combined PNO++ method with truncation of the PNO and PNO++ spaces, we plot the energies and specific rotations keeping one threshold, either $T_{\rm cutPNO}$ or $T_{\rm cutPNO++}$, constant at 10^{-6} while varying the other in Figures 7 and 8. We compare the results for correlation energies and specific rotations, selecting the best result from the previous section as a standard of comparison for each property. Thus, we compare CCSD-level correlation energies using the PNO method and dynamic polarizabilities and specific rotations using the PNO++ method.

A natural outcome of combining the spaces is that while fixing the orbitals obtained from one space, the convergence behavior follows that of the other space. For example, when keeping a fixed number of orbitals from the PNO space, the combined PNO++ follows the PNO++ method as we add orbitals from the PNO++ space. By comparing the leftmost point in the energy and rotation graphs, we can see that fixing the PNO++ threshold to 10^{-6} versus fixing the PNO threshold to 10^{-6} results in a larger space to begin with, due to larger numbers of orbitals being kept at the same threshold; however, this difference is effectively avoided by plotting against T_2 ratios, and the convergence behavior can be fairly compared.

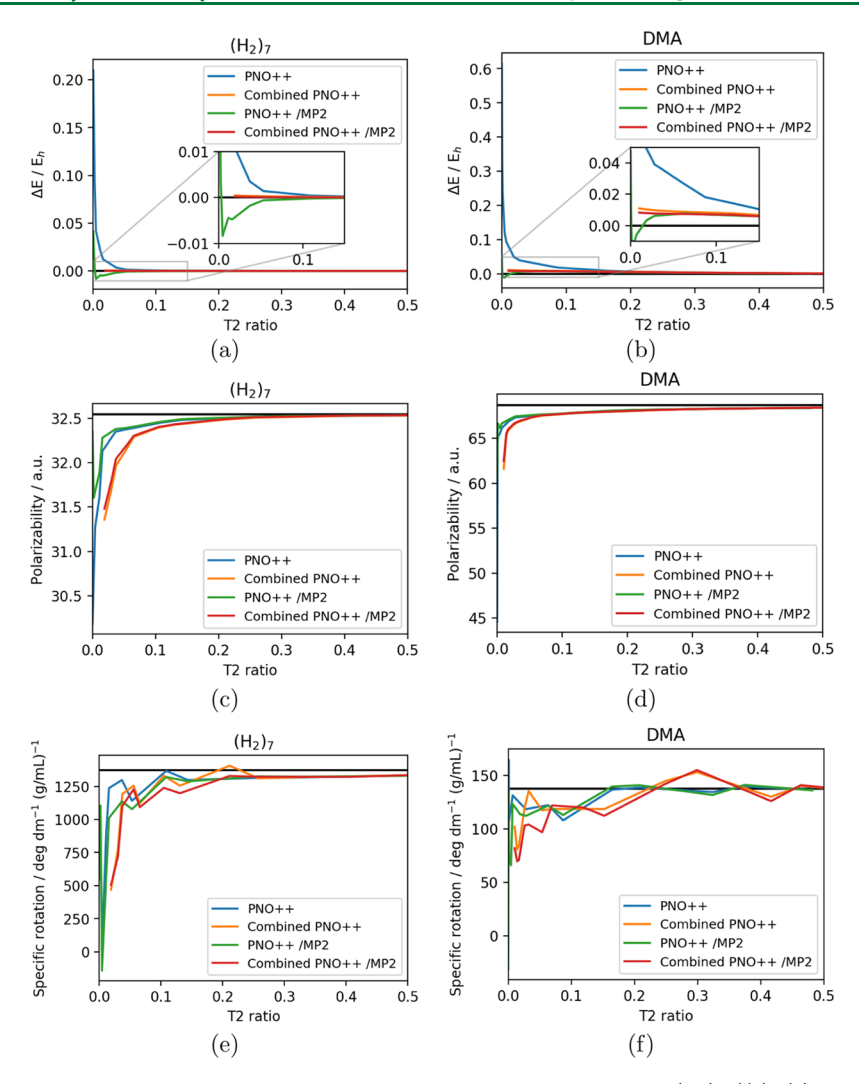


Figure 9. CCSD correlation energies, dynamic polarizabilties, and specific rotations at 589 nm for $(H_2)_7$ ((a), (c), and (e), respectively) and 1,3-dimethylallene (DMA) ((b), (d), and (f), respectively), computed using the aug-cc-pVDZ basis set.

When comparing the CCSD correlation energies in Figure 7, we see that while neither combined method has the quick convergence of the PNO method, fixing the $T_{\rm cutPNO}$ threshold brings us closer to the reference value than fixing the $T_{\rm cutPNO++}$ threshold at a given truncation. The addition of PNO++ orbitals does not improve the correlation energy as efficiently as the addition of PNO orbitals, causing a crossover point in all systems. Though the error in the energy computed using a fixed $T_{\rm cutPNO}$ is not seen to converge for $\rm H_2O_2$ and DMA Figure 7c,d at the largest T_2 ratios considered, the energy will converge to the full CCSD value as either of the thresholds $T_{\rm cutPNO}$ or $T_{\rm cutPNO++}$ are tightened.

Figure 8 shows the specific rotations computed using the same sets of spaces as Figure 7 but compared here to the PNO ++ data, which was seen in the previous section to converge to a value close to the reference relatively quickly for all systems. Once again, the combined methods show slower convergence; however, the combined method with the fixed number of unperturbed orbitals shows convergence behavior to within $\pm 14\%$ of the reference value at a T_2 ratio of 0.4 and higher for all systems. Thus, the convergence behavior of the method with the fixed $T_{\rm cutPNO}$ follows the PNO++ behavior, while the method with the fixed $T_{\rm cutPNO++}$ follows the nonconverging PNO behavior seen in Section 3.3.3. Thus, to achieve the well-

behaved convergence of specific rotation seen with the PNO+ + method, it is preferred to fix $T_{\rm cutPNO}$, in effect adding a fixed number of PNO orbitals to the PNO++ space.

3.5. MP2-Level Corrections. MP2-level corrections were computed for the PNO++ and combined PNO++ methods using the method described in Section 2.4. The goal of the MP2-level corrections was to recapture some of the accuracy lost due to the truncation of the PNO++ space, by adding in corrections computed as in eqs 14 and 15.

Figure 9 looks at the effect of corrections on the PNO++ and the combined PNO++ methods for the $(H_2)_7$ and DMA systems. As expected, the CCSD correlation energies are improved by the addition of MP2-level corrections; however, there is some tendency to overcorrect at very small T_2 ratios Figure 9a,b. The polarizability and rotation data in Figure 9c,d,e,f do not show a substantial improvement in accuracy at a given T_2 ratio on the addition of an MP2-level correction.

Adding corrections computed in this way at the MP2 level does not improve the description of the system's response to an external electromagnetic field. Since one normally computes coupled cluster linear response properties using converged coupled cluster amplitudes, and the corrections are computed using MP2-level amplitudes, it could be argued that simply adding the external field in the form of a perturbation to MP2-

level amplitudes does not take into account the sensitive nature of response properties.

4. CONCLUSIONS

In this work, we have examined a reduced-scaling approach optimized for response properties, computing truncation errors in CCSD correlation energies, dynamic polarizabilities, and specific rotations for a few test systems. This approach, dubbed PNO++, conserves the sparsity introduced into the wave function by the PNO approach, while also having a relatively diffuse orbital space, required for the accurate calculation of higher-order response properties. The PNO++ method is not, however, optimized for correlation energies and thus shows large truncation errors in the CCSD correlation energy at small fractions of the space. We find that incorporating a fixed number of orbitals from the PNO space into the PNO++ method recovers accuracy in the CCSD correlation energy. This combined PNO++ method allows for the truncation of a large portion of the space, up to a T_2 ratio of 0.5, without sacrificing accuracy in both the response property and the CCSD correlation energy. MP2-level corrections, while improving the value of the correlation energy at highlytruncated system sizes, do not improve the quality of the more sensitive dynamic polarizabilty and optical rotation at similarlytruncated sizes. A production-level implementation that includes screening for weak pairs as well as method-specific optimizations will be required to estimate the true computational savings obtained through truncation of the PNO++ space created using this form of perturbation-aware density for the computation of linear response properties.

ASSOCIATED CONTENT

Supporting Information

The Supporting Information is available free of charge at https://pubs.acs.org/doi/10.1021/acs.jctc.0c01086.

Molecular geometries used, CCSD energy, polarizability and specific rotation data for additional systems, comparisons of CCSD energy, polarizability, and specific rotation data for different representations of the electric dipole moment operator, PNO++ data using the magnetic dipole moment operator, and T_2 ratios as a function of $T_{\rm cut}$ thresholds (PDF)

■ AUTHOR INFORMATION

Corresponding Author

T. Daniel Crawford – Department of Chemistry, Virginia Tech, Blacksburg, Virginia 24061, United States; Molecular Sciences Software Institute, Blacksburg, Virginia 24060, United States; orcid.org/0000-0002-7961-7016; Email: crawdad@vt.edu

Author

Ruhee D'Cunha – Department of Chemistry, Virginia Tech, Blacksburg, Virginia 24061, United States

Complete contact information is available at: https://pubs.acs.org/10.1021/acs.jctc.0c01086

Notes

The authors declare no competing financial interest.

ACKNOWLEDGMENTS

This research was supported by the U.S. National Science Foundation (grant CHE-1900420). The authors are grateful to Dr. Ashutosh Kumar for helpful discussions and to Advanced Research Computing at Virginia Tech for providing computational resources and technical support that have contributed to the results reported within the paper.

REFERENCES

- (1) Helgaker, T.; Coriani, S.; Jørgensen, P.; Kristensen, K.; Olsen, J.; Ruud, K. Recent advances in wave function-based methods of molecular-property calculations. *Chem. Rev.* **2012**, *112*, 543–631.
- (2) Langhoff, P. W.; Epstein, S. T.; Karplus, M. Aspects of time-dependent perturbation theory. *Rev. Mod. Phys.* 1972, 44, 602–644.
- (3) Barron, L. D. Molecular Light Scattering and Optical Activity, 2nd ed.; Cambridge University Press: Cambridge, 2004.
- (4) Crawford, T. D. Ab initio calculation of molecular chiroptical properties. *Theor. Chem. Acc.* **2006**, *115*, 227–245.
- (5) Koch, H.; Jørgensen, P. Coupled-Cluster Response Functions. J. Chem. Phys. 1990, 93, 3333–3344.
- (6) Pedersen, T. B.; Koch, H. Coupled cluster response functions revisited. *J. Chem. Phys.* **1997**, *106*, 8059.
- (7) Olsen, J.; Jørgensen, P. Linear and nonlinear response functions for an exact state and for an MCSCF state. *J. Chem. Phys.* **1984**, 82, 3235–3264.
- (8) Jorgensen, P. Molecular and Atomic Applications of Time-Dependent Hartree-Fock Theory. *Annu. Rev. Phys. Chem.* **1975**, 26, 359–380.
- (9) Oddershede, J. Polarization Propagator Calculations. In *Advances in Quantum Chemistry*; Academic Press, 1978; Vol. 11, pp 275–352.
- (10) Casida, M. E. Recent Advances in Density Functional Methods, Part I; Chong, D. P., Ed.; World Scientific, 1995; Chapter 5, pp 155–192.
- (11) Casida, M. E. Time-dependent density-functional theory for molecules and molecular solids. *J. Mol. Struct.: THEOCHEM* **2009**, *914*, 3–18.
- (12) Nielsen, E. S.; Jørgensen, P.; Oddershede, J. Transition moments and dynamic polarizabilities in a second order polarization propagator approach. *J. Chem. Phys.* **1980**, *73*, 6238–6246.
- (13) Packer, M. J.; Dalskov, E. K.; Enevoldsen, T.; Jensen, H. J. A.; Oddershede, J. A new implementation of the second-order polarization propagator approximation (SOPPA): The excitation spectra of benzene and naphthalene. *J. Chem. Phys.* **1996**, *105*, 5886–5900.
- (14) Schirmer, J. Beyond the random-phase approximation: A new approximation scheme for the polarization propagator. *Phys. Rev. A* **1982**, *26*, 2395–2416.
- (15) Trofimov, A. B.; Krivdina, I. L.; Weller, J.; Schirmer, J. Algebraic-diagrammatic construction propagator approach to molecular response properties. *Chem. Phys.* **2006**, *329*, 1–10.
- (16) Dreuw, A.; Wormit, M. The algebraic diagrammatic construction scheme for the polarization propagator for the calculation of excited states. *Wiley Interdiscip. Rev. Comput. Mol. Sci.* 2015, 5, 82–95.
- (17) Čížek, J. On the Correlation Problem in Atomic and Molecular Systems. Calculation of Wavefunction Components in Ursell-Type Expansion Using Quantum-Field Theoretical Methods. *J. Chem. Phys.* **1966**, 45, 4256–4266.
- (18) Čížek, J. On the Use of the Cluster Expansion and the Technique of Diagrams in Calculations of Correlation Effects in Atoms and Molecules. *Adv. Chem. Phys.* **2007**, *XIV*, 35–89.
- (19) Sinanoglu, O. Many-electron theory of atoms, molecules and their interactions. *Adv. Chem. Phys.* **1964**, *6*, 315–412.
- (20) Crawford, T. D.; Schaefer, H. F. Reviews in Computational Chemistry; Lipkowitz, D. B. B., Ed.; John Wiley and Sons, Inc.: New York, 1995; Chapter 2, pp 33–136.
- (21) Saebo, S.; Pulay, P. Local Treatment Of Electron Correlation*. Annu. Rev. Phys. Chem. 1993, 44, 213–236.

- (22) Pulay, P. Localizability of dynamic electron correlation. *Chem. Phys. Lett.* **1983**, *100*, 151–154.
- (23) Hampel, C.; Werner, H.-J. Local treatment of electron correlation in coupled cluster theory. *J. Chem. Phys.* **1996**, *104*, 6286–6297.
- (24) Neese, F.; Wennmohs, F.; Hansen, A. Efficient and accurate local approximations to coupled-electron pair approaches: An attempt to revive the pair natural orbital method. *J. Chem. Phys.* **2009**, *130*, No. 114108.
- (25) Schütz, M.; Werner, H. J. Low-order scaling local electron correlation methods. IV. Linear scaling local coupled-cluster (LCCSD). *J. Chem. Phys.* **2001**, *114*, 661–681.
- (26) Yang, J.; Chan, G. K.-L.; Manby, F. R.; Schütz, M.; Werner, H.-J. The orbital-specific-virtual local coupled cluster singles and doubles method. *J. Chem. Phys.* **2012**, *136*, No. 144105.
- (27) Kinoshita, T.; Hino, O.; Bartlett, R. J. Singular value decomposition approach for the approximate coupled-cluster method. *J. Chem. Phys.* **2003**, *119*, 7756–7762.
- (28) Koch, H.; Sánchez De Merás, A.; Pedersen, T. B. Reduced scaling in electronic structure calculations using Cholesky decompositions. *J. Chem. Phys.* **2003**, *118*, 9481–9484.
- (29) Hohenstein, E. G.; Parrish, R. M.; Martínez, T. J. Tensor hypercontraction density fitting. I. Quartic scaling second- and third-order Møller-Plesset perturbation theory. *J. Chem. Phys.* **2012**, *137*, 1085.
- (30) Schutski, R.; Zhao, J.; Henderson, T. M.; Scuseria, G. E. Tensor-structured coupled cluster theory. *J. Chem. Phys.* **2017**, *147*, No. 184113.
- (31) Parrish, R. M.; Zhao, Y.; Hohenstein, E. G.; Martínez, T. J. Rank reduced coupled cluster theory. I. Ground state energies and wavefunctions. *J. Chem. Phys.* **2019**, *150*, No. 164118.
- (32) Pawłowski, F.; Olsen, J.; Jørgensen, P. Cluster perturbation theory. I. Theoretical foundation for a coupled cluster target state and ground-state energies. *J. Chem. Phys.* **2019**, *150*, No. 134108.
- (33) Gordon, M. S.; Fedorov, D. G.; Pruitt, S. R.; Slipchenko, L. V. Fragmentation methods: A route to accurate calculations on large systems. *Chem. Rev.* **2012**, *112*, 632–672.
- (34) Epifanovsky, E.; Zuev, D.; Feng, X.; Khistyaev, K.; Shao, Y.; Krylov, A. I. General implementation of the resolution-of-the-identity and Cholesky representations of electron repulsion integrals within coupled-cluster and equation-of-motion methods: Theory and benchmarks. *J. Chem. Phys.* 2013, 139, No. 134105.
- (35) Li, W.; Li, S. Divide-and-conquer local correlation approach to the correlation energy of large molecules. *J. Chem. Phys.* **2004**, *121*, 6649–6657.
- (36) Li, W.; Piecuch, P.; Gour, J. R.; Li, S. Local correlation calculations using standard and renormalized coupled-cluster approaches. *J. Chem. Phys.* **2009**, *131*, No. 114109.
- (37) Meyer, W. PNO-CI Studies of electron correlation effects. I. Configuration expansion by means of nonorthogonal orbitals, and application to the ground state and ionized states of methane. *J. Chem. Phys.* **1973**, 58, 1017–1035.
- (38) Edmiston, C.; Krauss, M. Pseudonatural orbitals as a basis for the superposition of configurations. I. He2+. *J. Chem. Phys.* **1966**, *45*, 1833–1839.
- (39) Edmiston, C.; Krauss, M. Pseudonatural Orbitals as a Basis for the Superposition of Configurations. II. Energy Surface for Linear H 3. *J. Chem. Phys.* **1968**, 49, 192–205.
- (40) Ahlrichs, R.; Driessler, F. Direct determination of pair natural orbitals. *Theor. Chim. Acta* **1975**, *36*, 275–287.
- (41) Neese, F.; Hansen, A.; Liakos, D. G. Efficient and accurate approximations to the local coupled cluster singles doubles method using a truncated pair natural orbital basis. *J. Chem. Phys.* **2009**, *131*, No. 064103.
- (42) Helmich, B.; Hättig, C. Local pair natural orbitals for excited states. J. Chem. Phys. 2011, 135, No. 214106.
- (43) Dutta, A. K.; Neese, F.; Izsák, R. Towards a pair natural orbital coupled cluster method for excited states. *J. Chem. Phys.* **2016**, *145*, No. 034102.

- (44) Peng, C.; Clement, M. C.; Valeev, E. F. State-Averaged Pair Natural Orbitals for Excited States: A Route toward Efficient Equation of Motion Coupled-Cluster. *J. Chem. Theory Comput.* **2018**, *14*, 5597–5607.
- (45) Frank, M. S.; Hättig, C. A pair natural orbital based implementation of CCSD excitation energies within the framework of linear response theory. *J. Chem. Phys.* **2018**, *148*, No. 134102.
- (46) Myhre, R. H.; Koch, H. The multilevel CC3 coupled cluster model. *J. Chem. Phys.* **2016**, *145*, No. 044111.
- (47) Korona, T.; Werner, H.-J. Local treatment of electron excitations in the EOM-CCSD method. *J. Chem. Phys.* **2003**, *118*, 3006–3019.
- (48) Kats, D.; Korona, T.; Schütz, M. Local CC2 electronic excitation energies for large molecules with density fitting. *J. Chem. Phys.* **2006**, *125*, No. 104106.
- (49) Gauss, J.; Werner, H. J. NMR chemical shift calculations within local correlation methods: The GIAO-LMP2 approach. *Phys. Chem. Chem. Phys.* **2000**, *2*, 2083–2090.
- (50) Kats, D.; Korona, T.; Schütz, M. Transition strengths and first-order properties of excited states from local coupled cluster CC2 response theory with density fitting. *J. Chem. Phys.* **2007**, 127, No. 064107.
- (51) Ledermüller, K.; Kats, D.; Schütz, M. Local CC2 response method based on the Laplace transform: Orbital-relaxed first-order properties for excited states. *J. Chem. Phys.* **2013**, *139*, No. 084111.
- (52) Schütz, M. Oscillator strengths, first-order properties, and nuclear gradients for local ADC(2). *J. Chem. Phys.* **2015**, *142*, No. 214103.
- (53) Russ, N. J.; Crawford, T. D. Local correlation in coupled cluster calculations of molecular response properties. *Chem. Phys. Lett.* **2004**, 400. 104–111.
- (54) McAlexander, H. R.; Mach, T. J.; Crawford, T. D. Localized optimized orbitals, coupled cluster theory, and chiroptical response properties. *Phys. Chem. Chem. Phys.* **2012**, *14*, 7830–7836.
- (55) McAlexander, H. R.; Crawford, T. D. A Comparison of Three Approaches to the Reduced-Scaling Coupled Cluster Treatment of Non-Resonant Molecular Response Properties. *J. Chem. Theory Comput.* **2016**, *12*, 209–222.
- (56) Kumar, A.; Crawford, T. D. Frozen virtual natural orbitals for coupled-cluster linear-response theory. *J. Phys. Chem. A* **2017**, *121*, 708–716.
- (57) Hóyvik, I. M.; Myhre, R. H.; Koch, H. Correlated natural transition orbitals for core excitation energies in multilevel coupled cluster models. *J. Chem. Phys.* **2017**, *146*, No. 144109.
- (58) Baudin, P.; Kristensen, K. LoFEx—A local framework for calculating excitation energies: Illustrations using RI-CC2 linear response theory. *J. Chem. Phys.* **2016**, *144*, No. 224106.
- (59) Baudin, P.; Kristensen, K. Correlated natural transition orbital framework for low-scaling excitation energy calculations (CorN-FLEx). *J. Chem. Phys.* **2017**, *146*, No. 214114.
- (60) Höfener, S.; Klopper, W. Natural transition orbitals for the calculation of correlation and excitation energies. *Chem. Phys. Lett.* **2017**, *679*, 52–59.
- (61) Mester, D.; Nagy, P. R.; Kállay, M. Reduced-cost linear-response CC2 method based on natural orbitals and natural auxiliary functions. *J. Chem. Phys.* **2017**, *146*, No. 194102.
- (62) Mester, D.; Nagy, P. R.; Kállay, M. Reduced-cost second-order algebraic-diagrammatic construction method for excitation energies and transition moments. *J. Chem. Phys.* **2018**, *148*, No. 094111.
- (63) Monkhorst, H. J. Calculation of properties with the coupled-cluster method. *Int. J. Quantum Chem.* 1977, 12, 421–432.
- (64) Dalgaard, E.; Monkhorst, H. J. Some aspects of the time-dependent coupled-cluster approach to dynamic response functions. *Phys. Rev. A* **1983**, 28, 1217–1222.
- (65) Mukherjee, D.; Mukherjee, P. A response-function approach to the direct calculation of the transition-energy in a multiple-cluster expansion formalism. *Chem. Phys.* **1979**, *39*, 325–335.

- (66) Rosenfeld, L. Quantenmechanische Theorie der naturlichen optischen Aktivitaet von Fluessigkeiten und Gasen. Z. Phys. 1929, 52, 161–174.
- (67) Møller, C.; Plesset, M. S. Note on an Approximation Treatment for Many-Electron Systems. *Phys. Rev.* **1934**, *46*, 618–622.
- (68) Bartlett, R. J.; Silver, D. M. Pair-correlation energies in sodium hydride with many-body perturbation theory. *Phys. Rev. A* **1974**, *10*, 1927–1931.
- (69) Boys, S. F. Construction of Some Molecular Orbitals to Be Approximately Invariant for Changes from One Molecule to Another. *Rev. Mod. Phys.* **1960**, 32, 296–299.
- (70) Pipek, J.; Mezey, P. G. A fast intrinsic localization procedure applicable for ab initio and semiempirical linear combination of atomic orbital wave functions. *J. Chem. Phys.* **1989**, *90*, 4916–4926.
- (71) Edmiston, C.; Ruedenberg, K. Localized Atomic and Molecular Orbitals. *Rev. Mod. Phys.* **1963**, *35*, 457–465.
- (72) Magnasco, V.; Perico, A. Uniform Localization of Atomic and Molecular Orbitals. I. J. Chem. Phys. 1967, 47, 971–981.
- (73) von Niessen, W. Density Localization of Atomic and Molecular Orbitals. I. *J. Chem. Phys.* **1972**, *56*, 4290–4297.
- (74) Hansen, A.; Liakos, D. G.; Neese, F. Efficient and accurate local single reference correlation methods for high-spin open-shell molecules using pair natural orbitals. *J. Chem. Phys.* **2011**, *135*, No. 214102.
- (75) Krause, C.; Werner, H.-J. Comparison of explicitly correlated local coupled-cluster methods with various choices of virtual orbitals. *Phys. Chem. Phys.* **2012**, *14*, 7591–7604.
- (76) Liakos, D. G.; Hansen, A.; Neese, F. Weak molecular interactions studied with parallel implementations of the local pair natural orbital coupled pair and coupled cluster methods. *J. Chem. Theory Comput.* **2011**, *7*, 76–87.
- (77) Riplinger, C.; Pinski, P.; Becker, U.; Valeev, E. F.; Neese, F. Sparse maps A systematic infrastructure for reduced-scaling electronic structure methods. II. Linear scaling domain based pair natural orbital coupled cluster theory. *J. Chem. Phys.* **2016**, 144, No. 024109.
- (78) Clement, M. C.; Zhang, J.; Lewis, C. A.; Yang, C.; Valeev, E. F. Optimized Pair Natural Orbitals for the Coupled Cluster Methods. *J. Chem. Theory Comput.* **2018**, *14*, 4581–4589.
- (79) Helmich, B.; Hättig, C. A pair natural orbital implementation of the coupled cluster model CC2 for excitation energies. *J. Chem. Phys.* **2013**, *139*, No. 084114.
- (80) Helmich, B.; Hättig, C. A pair natural orbital based implementation of ADC(2)-x: Perspectives and challenges for response methods for singly and doubly excited states in large molecules. *Comput. Theor. Chem* **2014**, 1040–1041, 35–44.
- (81) Dutta, A. K.; Nooijen, M.; Neese, F.; Izsák, R. Exploring the Accuracy of a Low Scaling Similarity Transformed Equation of Motion Method for Vertical Excitation Energies. *J. Chem. Theory Comput.* **2018**, *14*, 72–91.
- (82) Dutta, A. K.; Saitow, M.; Riplinger, C.; Neese, F.; Izsák, R. A near-linear scaling equation of motion coupled cluster method for ionized states. *J. Chem. Phys.* **2018**, *148*, No. 244101.
- (83) Datta, D.; Kossmann, S.; Neese, F. Analytic energy derivatives for the calculation of the first-order molecular properties using the domain-based local pair-natural orbital coupled-cluster theory. *J. Chem. Phys.* **2016**, *145*, No. 114101.
- (84) Crawford, T. D.; Kumar, A.; Bazanté, A. P.; Di Remigio, R. Reduced-scaling coupled cluster response theory: Challenges and opportunities. *Wiley Interdiscip. Rev. Comput. Mol. Sci.* **2019**, *9*, 1–25.
- (8S) Shavitt, I.; Bartlett, R. J. Many-Body Methods in Chemistry and Physics: MBPT and Coupled-Cluster Theory; Cambridge Molecular Science; Cambridge University Press, 2009.
- (86) Woon, D. E.; Dunning, T. H. Gaussian basis sets for use in correlated molecular calculations. III. The atoms aluminum through argon. *J. Chem. Phys.* **1993**, 98, 1358–1371.